Available online at www.sciencedirect.com
SCIENCE DIRECT®
PERGAMON
International Journal of Heat and Mass Transfer 46 (2003) 3201–3209
International Journal of HEAT and MASS TRANSFER
www.elsevier.com/locate/ijhmt

Estimation of particle volume fraction, mass fraction and number density in thermophoretic deposition systems

Pushkar Tandon *, James P. Terrell, Xiaodong Fu, Amy Rovelstad

Corning Inc., SP-DV-01, Corning, NY 14831, USA

Received 26 April 2002; received in revised form 2 February 2003

Abstract

A method is presented to predict the soot volume fraction in soot-laden gas streams in systems where thermophoresis is the dominant mechanism of particle deposition onto adjoining surfaces. In particular, we considered deposition of silica particles on a circular cylinder in cross-flow to a premix CH_4/O_2 flame, a setup similar to the one used in the outside vapor deposition process used for making optical fibers. Silica particles were produced by introducing $SiCl_4$ along with the premix gases to the burner and were collected on a cylinder. Heat flux and mass deposition rate measurements on the cylinder were performed and recorded as a function of time. Considering thermophoresis to be the dominant mechanism of particle deposition, a simple theory was developed to establish the relationship between the measured quantities. The theory predicted that the thickness at any given time t was expected to increase linearly with the integral of $q''(t)\,dt$ (integrated from $t = 0$ to $t = t$), where $q''(t)$ is the heat flux. Such a linear relationship was observed for five different reactant flow rates confirming thermophoresis to be the dominant mechanism of particle deposition. Soot volume fraction and soot mass fraction were calculated from the slope of these linear fits and were seen to be in good agreement with the estimates of the soot fraction from light scattering measurements. Based on the light scattering estimates of particle diameter, particle number densities were also estimated.

Keywords: Heat flux; Particle mass deposition rate; Thermophoresis; Volume fraction; Particle number density

1. Introduction

Deposition of particles from flowing suspensions to adjoining surfaces is important in many engineering applications. Thermophoresis is the dominant mechanism of particle deposition in a number of systems of practical interest where highly non-isothermal environment exists. Thermophoresis is a phenomenon, which describes the tendency of particles to migrate in the direction of decreasing gas temperature (see e.g. [1,2]). This phenomena has been extensively studied in the literature. Brock [1,2] and Talbot et al. [3] have developed expressions for the thermophoretic force for continuum, transition and Knudsen regimes. Goren [4] studied the thermophoretic behavior of aerosol particles in the laminar boundary layer on a flat plate. Batchelor and Shen [5] and Shen [6] predicted thermophoretic deposition of particles onto cold surfaces in two-dimensional and axisymmetric flows. Homsy et al. [7] and Walker et al. [8] have developed analytical expressions for the thermophoretic deposition rates in laminar tube and other boundary layer flows.

Thermophoresis has been known to be the dominant mechanism of particle deposition in different techniques used for making optical fibers [9,10]. Numerical simulations for the outside vapor deposition (OVD) process have been done by Hong and Kang [11], Cho et al. [12] and Wu and Greif [13]. The OVD process involves generation of pyrogenic silica/doped silica particles in a flame and then targeting and depositing them on a rotating cylindrical target rod. Similar analysis for the

* Corresponding author. Tel.: +1-607-974-2933; fax: +1-607-974-9271.
E-mail address: tandonp@corning.com (P. Tandon).

0017-9310/03/$ - see front matter © 2003 Elsevier Science Ltd. All rights reserved.
doi:10.1016/S0017-9310(03)00117-0

Nomenclature

$c_{p,p}$	particle heat capacity
D_p	Brownian diffusivity
d_w	cylinder diameter
d_{TC}	thermocouple bead diameter
h	thickness
j''	mass flux
k_g	thermal conductivity of the gas
N_p	particle number density
Nu_h	Nusselt number
Pr	Prandtl number
q''	heat flux
Re_D	Reynolds number based on cylinder diameter
Re	Reynolds number based on thermocouple bead diameter
T	temperature
T_w	deposit surface temperature
T_{TC}	thermocouple temperature
T_s	surrounding temperature
V_T	thermophoretic velocity

Greek symbols

α_T	thermophoretic diffusion coefficient
α_{mom}	momentum accomodation coefficient
α_p	particle thermal accomodation coefficient
ε_w	surface emissivity
ϕ	soot volume fraction
γ	ratio of heat flux by soot deposition and by the impinging flame
κ	exponent with which thermal conductivity of gas increases with temperature
ν	momentum diffusivity
ρ_p	particle density
ρ_d	deposit density
ρ_g	gas density
σ	Stefan–Boltzmann constant
ω	mass fraction

Subscripts

e	properties calculated at gas temperature T_g
p	particle
g	gas

modified chemical vapor deposition (MCVD) process has also been reported by Park et al. [14], Park and Choi [15,16] and Kim and Pratsinis [17]. In the MCVD process, reactants are flown inside a glass tube as the tube is heated by a traversing flame from the outside. The reactants form particles in the tube and deposit on the inside of the tube. Most of the studies outlined above have theoretically treated the problem of thermophoretic deposition, while very few experiments have been reported. Graham and Alam [18] experimentally measured preform temperature, deposition efficiency and particle size distribution for a OVD system. Bautista et al. [19] have attempted to explain the deposition efficiency data for the OVD process using extensions of the thermophoretic deposition model of Homsy et al. [7] and an assumed target temperature. We have here carried out deposition rate and heat flux measurements to demonstrate that thermophoresis is the dominant mechanism of particle deposition in the OVD process. In particular, we considered deposition of silica particles on a circular cylinder in cross-flow to a premix CH_4/O_2 flame, a setup similar to the one used in the OVD process used for making optical fibers. Since the thermophoretic deposition rate and the heat flux are both proportional to the gradient of temperature, a simple theory was developed which established a quantitative relationship between the particle deposition rate and heat flux. Motivated by this theory, soot deposit thickness and heat flux were measured at the stagnation point of a circular cylinder in cross-flow to a CH_4/O_2 premix flame. Temperature measurements were also performed in the flame, at a height equal to the distance between the cylinder and the burner, using a B-type thermocouple and were corrected for radiation losses. Based on these measurements, we found that the rate of particle deposition was linearly proportional to the heat flux, confirming thermophoresis to be the mechanism of particle transport to the surface. Moreover, the theory was used to estimate the soot volume fraction in the gas stream from the slope of the linear relationship between the deposition rate and the heat flux. Independent measurements of the soot volume fraction were also performed using the static light scattering technique and the predictions from the two techniques were in good agreement. For these values of soot volume fraction and using the soot mean diameter estimated from the light scattering experiments, soot number densities in the gas stream were also calculated. The approach outlined here is similar to the one used by Eisner and Rosner [20] and McEnally et al. [21], where they used temperature response data of a thermocouple to determine the flame volume fraction. However, by directly measuring the heat flux on the target, we avoid the issues involved with smoothing of the temperature response data for it to be processed or assuming a correlation for obtaining heat flux from thermocouple data.

2. Methods

2.1. Theory

2.1.1. Principal assumptions

To capture the essential features of thermophoretic deposition of particles on a cylinder in cross-flow to a methane-oxygen flame, our analysis is based on the following assumptions:

(a) Thermophoresis is the dominant mechanism of particle deposition. There is some inertial contribution to the deposition rate [22] for high mass loading systems, but this contribution has been estimated to be less than 20% [23]. Water cooling of the metal cylinder further enhances the thermophoretic contribution to the particle flux at the cylinder.
(b) Brownian diffusion of particles is neglected. The effect on the deposition rate due to the thin "Brownian" sub-layer adjacent to the target [4] is considered to be negligible.
(c) Conduction and convection are the dominant mechanisms of heat transfer from the flame to the target. Radiation from the soot to the cylinder or from the cylinder to the surroundings has been neglected.
(d) Depositing particles do not transfer appreciable heat from the flame to the target. The ratio of heat flux by soot deposition and by the impinging flame, γ, is estimated to be:

$$\gamma = \frac{q''_{\mathrm{p}}}{q''_{\mathrm{f}}} = \left\{ \frac{(\alpha_{\mathrm{T}} D_{\mathrm{p}})_{\mathrm{e}} \rho_{\mathrm{p}} \phi_{\mathrm{p}} \langle \alpha_{\mathrm{p}} \rangle c_{\mathrm{p,p}} (T_{\mathrm{p,e}} - T_{\mathrm{w}})}{k_{\mathrm{g,e}} T_{\mathrm{g}}} \right\} \frac{1}{1-\omega_{\mathrm{e}}} \quad (1)$$

where $(\alpha_{\mathrm{T}} D_{\mathrm{p}})$ is the thermophoretic diffusivity, T_{w} is the deposit surface temperature, T_{g} is the flame temperature, ρ_{p} is the density of the soot particles, ϕ_{p} is the soot volume fraction, $\langle \alpha_{\mathrm{p}} \rangle$ is the particle thermal accommodation coefficient, $c_{\mathrm{p,p}}$ is the soot heat capacity, $T_{\mathrm{p,e}}$ is the particle temperature outside of the boundary layer, ω_{e} is the soot mass fraction, $k_{\mathrm{g,e}}$ is the gas phase thermal conductivity and subscript e correspond to the properties calculated at temperature T_{g}. For our system, this fraction was calculated to be less than 0.03.
(e) No appreciable soot nucleation takes place in the thermal boundary layer adjacent to the target. Most of the particle nucleation takes place far upstream in the flame.
(f) It is assumed that the heat flux sensor location on the cylinder is completely covered with soot within first 5–6 s of exposure to the soot-laden flame. This allowed us to extrapolate the tail of the heat flux curve for times >6 s. The heat flux measurements were not performed for longer times because the maximum service temperature of the sensor face was 600 °C.
(g) Since the thickness of the deposit formed during the heat flux measurements is small, it is considered that the heat flux to the original target surface (sensor) is equal to the heat flux at the depositing surface. We have developed methods to estimate the time dependent relationship between heat flux on the surface of the original target and heat flux at the deposit surface for thick deposits (including effects due to rotating target and traversing flame), details of which will be presented in Tandon and Balakrishnan [24].
(h) The soot thickness is much smaller than the cylinder radius.
(i) Multiple scattering events are neglected in estimating the number densities from the light scattering data.
(j) A quasi-steady conduction–convection–radiation energy balance can be used to estimate the radiation correction to the thermocouple measurements [20].

2.1.2. Mathematical model

The particle thermophoretic drift velocity, V_{T}, is given as [25,26]:

$$V_{\mathrm{T}} = (\alpha_{\mathrm{T}} D_{\mathrm{p}}) \left(-\frac{\mathrm{grad}\, T}{T} \right) \quad (2)$$

where α_{T} is the thermophoretic diffusion factor, D_{p} is the particle Brownian diffusivity, T is the local gas temperature and grad T its local spatial gradient. From Eq. (2), the thermophoretic deposition mass flux on a circular cylindrical in cross-flow to a soot-laden stream is calculated as [20]:

$$j'' = (\alpha_{\mathrm{T}} D_{\mathrm{p}})_{\mathrm{e}} \frac{Nu_{\mathrm{h}}}{d_{\mathrm{w}}} \frac{1}{1+\kappa} \left[1 - \left(\frac{T_{\mathrm{w}}}{T_{\mathrm{g}}} \right)^{1+\kappa} \right] \rho_{\mathrm{p}} \phi_{\mathrm{p,e}} \quad (3)$$

where ϕ_{p} is the soot volume fraction, ρ_{p} is the density of the soot particles, κ is the exponent with which gas stream thermal conductivity increases with the gas temperature, Nu_{h} is the orientation averaged Nusselt number for heat transfer, d_{w} is the cylinder diameter, T_{w} is the deposit surface temperature, T_{g} is the mainstream gas temperature outside the thermal boundary layer and subscript e corresponds to the properties calculated at T_{g}. The thermophoretic flux expression given by Eq. (3) takes into account the effect of temperature dependent gas properties in the thermal boundary layer. Similarly, heat flux to the cylinder is calculated as [20,27]:

$$q'' = k_{\mathrm{g,e}} T_{\mathrm{g}} \frac{Nu_{\mathrm{h}}}{d_{\mathrm{w}}} \frac{1}{1+\kappa} \left[1 - \left(\frac{T_{\mathrm{w}}}{T_{\mathrm{g}}} \right)^{1+\kappa} \right] \quad (4)$$

where k_{g} is the gas thermal conductivity. Exploiting the relation:

$$j'' = \rho_d \frac{d}{dt}\left(\frac{d_w}{2}\right) = \rho_d \frac{dh}{dt} \quad (5)$$

Eqs. (3) and (4) are combined to give:

$$h(t) = \left[\frac{(\alpha_T D_p)_e \phi_{p,e} \rho_p}{T_g k_{g,e} \rho_d}\right] \int_0^t q''(t)\,dt \quad (6)$$

where $h(t)$ is the deposit thickness and ρ_d is the density of the deposit. Thus, if thermophoresis is the mechanism of particle transport to the surface, we expect a plot of measured $h(t)$ vs. the integral of the RHS of Eq. (6) (calculated based on measured heat flux data) to be a straight line with the slope equal to the expression in the square bracket. The thermophoretic diffusion coefficient, $\alpha_T D_p$, in the free-molecular regime is calculated as [26,28]:

$$\alpha_T D_p = \left(\frac{3}{4}\right)\left[1 + \left(\frac{\pi \alpha_{mom}}{8}\right)\right]^{-1} v \quad (7)$$

where α_{mom} is the tangential momentum accomodation coefficient (taken to be 0.9 [25,26,28] and v is the momentum diffusivity of the local gas mixture.

2.2. Experiments

2.2.1. Particle generation and deposition

Silica particles were generated in a methane-oxygen flame by introducing $SiCl_4$ as the precursor to the burner using a bubbler. $SiCl_4$ oxidized in the flame to give rise to silica particles [29,30], which then grew by aggregation and vapor scavenging as they were transported and deposited on the cylinder. Experiments were done for different combinations of oxidizer, fuel and precursor flow rates and heat flux and growth rate measurements were performed. Static light scattering experiments were also performed for the same set of conditions and the results from the two techniques were compared.

2.2.2. Heat flux measurements

In Fig. 1, we show a schematic of the experimental setup used to collect the heat flux data. The experimental set-up consisted of a stainless steel cylinder, 8″ long with a 4″ outside diameter and 0.5″ wall thickness. A thin-film heat flux sensor [31] manufactured by Vatell Corporation was imbedded in the wall of the cylinder at the mid-point. The top face of the sensor consisted of a thin-film (~2 μm thick) deposited differential thermopile and an independent thin-film resistive temperature sensor (RTS). The diameter of the sensor was 0.25″ and was mounted such that the active flat face was virtually flush with the cylinder surface to minimize flow disruptions. Flame temperatures exceeded 2000 K. However, since the maximum service temperature of the sensor face was 600 °C, the sensor housing was water-cooled to maximize sensor life. The water temperature was maintained at 23 °C by a Neslab water chilling unit. The $SiCl_4$ bubbler temperature was maintained using a PID controller. A high temperature baffle was attached to the cylinder to serve as a shutter between the sensor and the flame. This allowed the sensor to remain unexposed to the flame between runs to ensure consistent initial thermal conditions for each run and to allow removal of the deposited soot from the previous run. To initiate a run, the cylinder was rotated by a stepper motor from the shuttered position to an orientation where the sensor was positioned at the stagnation point of the flame. The sensor remained at the stagnation position for approximately 5 s before the cylinder was rotated back to the shuttered position. Simultaneous heat flux and sensor face temperature data was acquired at a sampling rate of 1000 Hz by an IBM Think Pad lap-top computer using a National Instruments 16 bit data acquisition card. The shutter events are evident in the heat flux plots shown in Fig. 2. This process was repeated for five flow conditions for a burner to sensor distance of 5″.

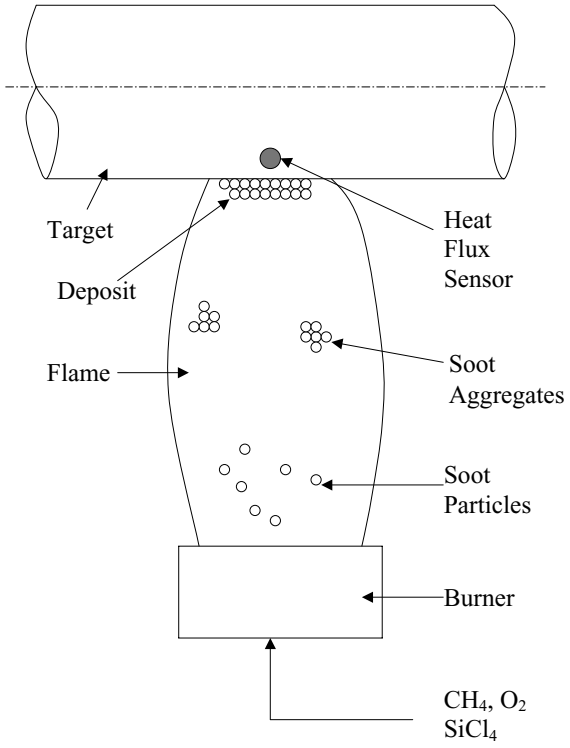

Fig. 1. Experimental setup for heat flux and deposition rate measurements.

2.2.3. Soot deposition rate measurements

The same experimental set-up used to acquire heat flux data was also used to collect soot deposition rates. The conditions used for the heat flux experiment were duplicated for the soot collection experiment. These in-

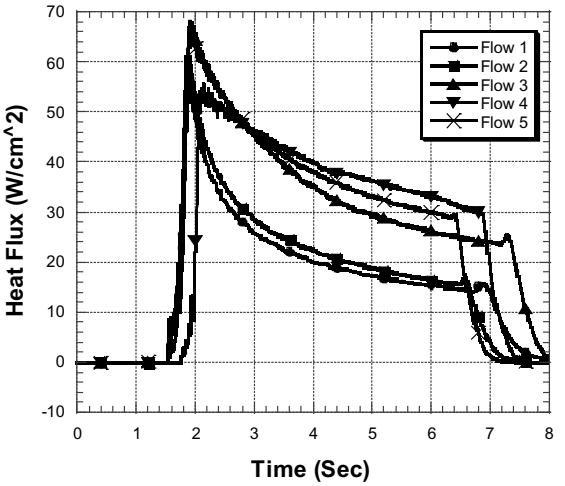

Fig. 2. Heat flux measurements at the forward stagnation point of a circular metal cylinder in cross-flow to a premix flame for five different flow conditions.

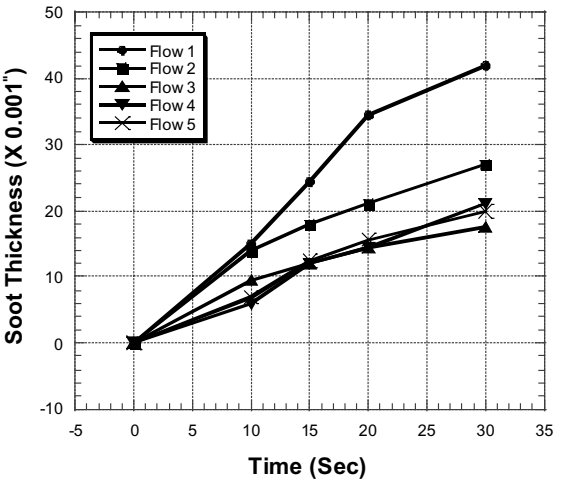

Fig. 3. Evolution of deposit thickness with time for different flow conditions.

clude water cooling temperature, bubbler temperature, burner to sensor distance and stepper motor angular velocity. The soot collection experiments were performed at a burner to sensor distance of 5″. For this experiment, the sensor was left in the stagnation position of the flame for 10, 15, 20 and 30 s intervals respectively. These exposure times were repeated for each set of burner flow conditions. After each run when the sensor was in the shuttered position, the soot deposited on the sensor face during the exposed time was carefully removed and the thickness measured and recorded to the nearest thousandth of an inch. The entire surface surrounding the sensor was then cleaned prior to the next run. The soot deposition rates are shown in Fig. 3.

2.2.4. Temperature measurements

Temperature measurements were performed by direct insertion of a B-type thermocouple in the flame at 5″ from the burner. The measured temperatures were corrected for radiation cooling using the procedure described in Eisner and Rosner [20]. Considering that the bead was spherical, a quasi-steady energy balance is given as:

$$\frac{k_{g,e}T_g(2\{1+(RePr/4)\})}{d_{TC}}\frac{1}{1+\kappa}\left[1-\left(\frac{T_{TC}}{T_g}\right)^{1+\kappa}\right] = \varepsilon_w\sigma_B(T_{TC}^4-T_s^4) \quad (8)$$

where the left hand side represents convective heat flux through a boundary layer with variable thermophysical properties and the right hand side is the radiative flux. In the above equation $k_{g,e}$ is the thermal conductivity of the host gas mixture at the gas temperature, T_g, T_{TC} and T_s are the gas, thermocouple and surrounding temperature respectively, d_{TC} is the bead diameter, Re is the Reynolds number calculated on the basis of thermocouple bead diameter, Pr is the gas Prandtl number, κ is the temperature exponent with which the thermal conductivity scales with temperature ($\kappa = d\ln k_{g,e}/d\ln T_g$), ε_w is the surface emissivity and σ_B is the Stefan–Boltzmann constant. Eq. (8) was used iteratively to calculate the radiation corrected gas temperature (T_g) from the thermocouple (T_{TC}) data.

2.2.5. Light scattering measurements

The silica soot particles generated in the flame were analyzed by measuring the scattering intensities obtained from their interaction with a polarized argon ion (514 nm) laser. Part of the light beam produced by the laser was passed through the flame and interacted with the silica soot particles. Two detectors placed at 20° (forward scatter) and 160° (backward scatter) recorded the scattering intensities of the silica soot particles. The ratio of the scattering intensities at these two complementary angles (often referred to as the method of *dissymmetry ratio* in the literature) turns out to be a function of mean particle diameter only [32–35]. Laws governing Mie scattering intensity [36] at angular position θ of a single particle of size d_p, refractive index μ and for light wavelength λ were used to calculate the mean particle diameter from the ratio of the scattering intensities at the two angles. The number density of the suspended particles was estimated from the ratio of the total scattered light measured to the theoretical scattering intensity expected from a single particle. In the above calculations, we neglected multiple scattering events and considered light scattering from N particles to be sum of light scattered from individual particles. Soot volume fraction estimates from static light

scattering measurements were compared with the corresponding measurements from the heat flux method.

3. Results and discussion

In Fig. 2, we show the heat flux measurements on the surface of the metal cylinder for five different flow rates. The heat flux was seen to decrease rapidly initially and then more gradually as a result of the growth of deposit on the surface. For the purposes of integrating the flux over time $t > 6$ s, the tail of the curves was extrapolated, assuming that a sufficiently thick soot layer was already deposited by then. The corresponding evolution of deposit thickness with time is shown in Fig. 3 (the units "mils" correspond to thousandths of an inch). The deposit thickness was plotted against the integral of heat flux over time and such a plot yielded a straight line for all the flow rates (Figs. 4–8), confirming thermophoresis to be the dominant mechanism of soot deposition. The slope of such a linear fit was used to estimate the soot volume fraction in the flame and the calculated values are reported in Table 2. These estimates were in very good agreement with the earlier estimates of soot volume fraction in the OVD process (see e.g. [22,23]) and the light scattering measurements described below. For

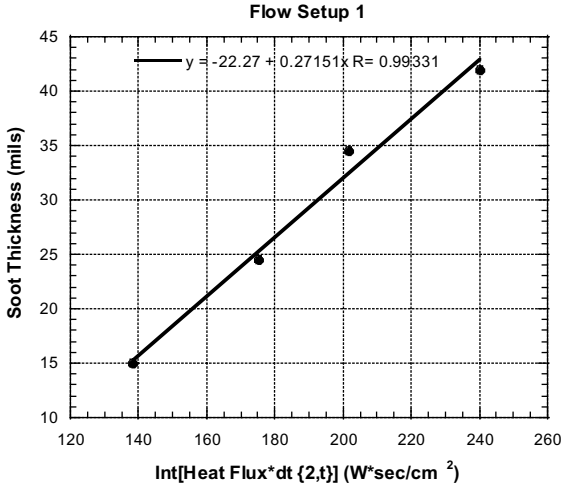

Fig. 4. Soot thickness vs. integral of heat flux over time for flow setup 1.

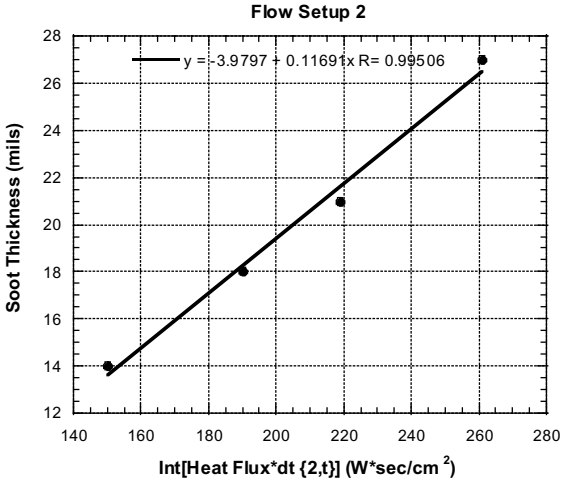

Fig. 5. Soot thickness vs. integral of heat flux over time for flow setup 2.

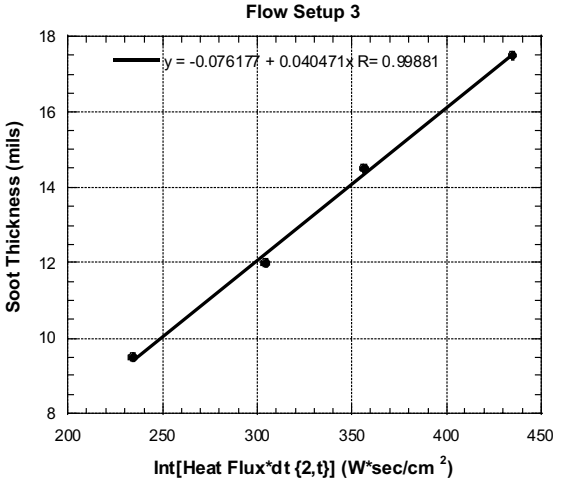

Fig. 6. Soot thickness vs. integral of heat flux over time for flow setup 3.

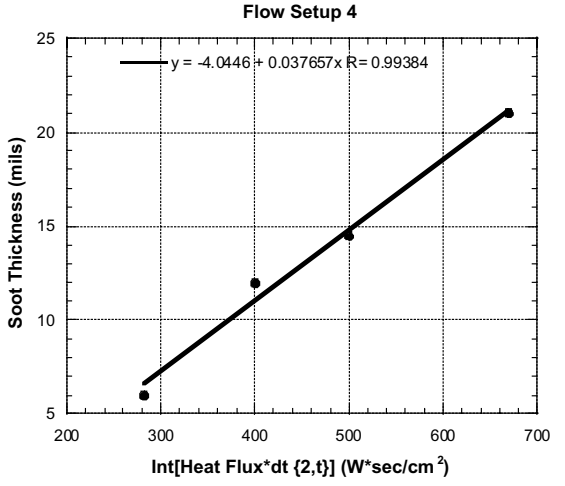

Fig. 7. Soot thickness vs. integral of heat flux over time for flow setup 4.

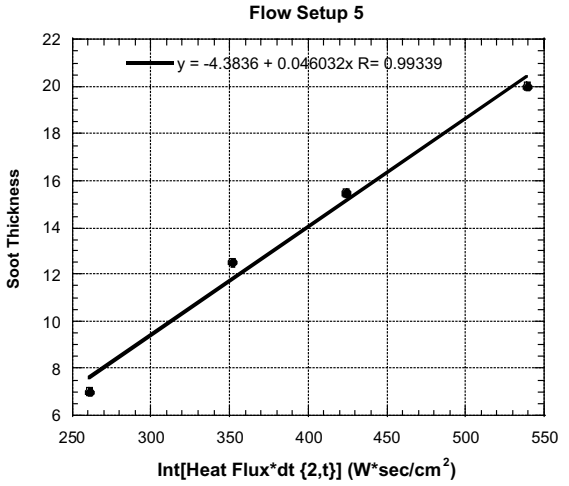

Fig. 8. Soot thickness vs. integral of heat flux over time for flow setup 5.

Table 1
Temperature measurements in the flame at a distance of 5″ from the burner for different flow rates

Flow setup	Radiation corrected temperature (K)
1	2017
2	1618
3	2186
4	1791
5	1890

each of the flow setups, the temperature in the flame at 5″ from the burner was measured using a B-type thermocouple and corrected for radiation cooling (Table 1). The temperature dependent gas properties of "combustion" gases were calculated using the following relations:

$$k_g = 1.62 \times 10^{-4}(T/1000) \quad \text{cal/cm s K}$$
$$v = 2.4(T/1000)^{1.7} \quad \text{cm}^2/\text{s} \tag{9}$$

The densities of soot particles and the soot layer were taken to be 2.2 and 0.5 g/cm^3 respectively. The soot mass fraction, ω, was estimated from the soot volume fraction using the approximate relation:

$$\frac{\omega}{1-\omega} \approx \frac{\phi \rho_p}{\rho_g} \tag{10}$$

where ρ_g is the gas density. The soot number density, N_p, was calculated as:

$$N_p = \frac{6\phi}{\pi d_p^3} \tag{11}$$

where the particle mean diameter, d_p, was estimated from light scattering experiments. The calculated soot mass fraction and number density are reported in Table 2, where we also present the calculated number densities for the different flow setups using light scattering experiments. The two techniques gave soot number densities, which were in good agreement with each other, with the exception of flow setup 1.

Light scattering is a standard technique for getting soot characteristics in soot-laden flows and flames. However, the method presented here has some advantages. The heat flux method presented here is rather inexpensive compared to the light scattering method. Moreover, light scattering is a difficult technique to use close to a target since scattered light from the suspended particles can be blocked by the target. This is precisely the location where knowing soot volume fraction is critical for "deposition efficiency" considerations. It is also not always easy to set-up light scattering measurements in most engineering systems of practical interest.

For calculating the soot volume fraction by the technique outlined here, it is assumed that thermophoresis is the dominant mechanism of particle deposition. However, for high loading systems, thermophoretic deposition is somewhat coupled with the inertial deposition of particles [22,37]. The inertial contribution is due to high particle mass loading [23] and not because of particle Stokes number being greater than the critical Stokes number [38]. Methods presented here will be refined in future to include effects due to inertia for improved estimates of soot volume fraction. In estimating the particle deposition rates, we have considered that the soot population with a particle size distribution can be

Table 2
Estimated values of soot volume fraction, soot mass fraction and soot number density from the slopes in Figs. 4–8

Flow setup	Soot volume fraction $\times 10^5$	Soot mass fraction	Soot number density $\times 10^{-9}$ (#/cm^3)	Soot mean diameter (μm): light scattering	Soot number density $\times 10^{-9}$ (#/cm^3): light scattering
1	9.94	0.55	23.73	0.194	3.96
2	4	0.287	9.549	0.215	6.06
3	1.5	0.17	3.58	0.272	3.89
4	1.33	0.129	3.174	0.175	5.55
5	1.655	0.163	3.95	0.201	4.68

represented by a volume-equivalent mean particle diameter. The assumption is justified since the thermophoretic diffusivity in the free-molecular regime is insensitive to particle size and structure [25,39]. However, the particle size distribution will effect the inertial contribution to the thermophoretic flux.

4. Conclusions

We have here presented a novel method to estimate soot volume fraction, mass fraction and number density in the gas stream from heat flux, mass deposition rate and temperature measurements in systems where thermophoresis is the dominant mechanism of deposition. We have implemented this scheme to estimate the soot volume fraction at 5″ from the burner by measuring the heat flux and deposition rate at the stagnation point on a metal cylinder in cross-flow to a CH_4/O_2 premix flame. For five sets of flow conditions, mass deposition rate was seen to be linearly proportional to the heat flux confirming thermophoresis to be the dominant mechanism of particle deposition. Soot volume fraction were calculated from the slope of these linear fits. Light scattering experiments for these flow conditions were also performed and particle number densities and mean diameter were estimated. The estimated values of soot volume fraction, mass fraction and number density from the heat flux measurements were in good agreement with the ones obtained from light scattering experiments.

References

[1] J.R. Brock, On the theory of thermal forces acting on aerosol particles, J. Colloid Interface Sci. 17 (1962) 768–780.
[2] J.R. Brock, The thermal force in the transition region, J. Colloid Interface Sci. 23 (1967) 448–452.
[3] L. Talbot, R.K. Cheng, R.W. Schefer, D.R. Willis, Thermophoresis of particles in a heated boundary layer, J. Fluid Mech. 101 (1980) 737–758.
[4] S.L. Goren, Thermophoresis of aerosol particles in the laminar boundary layer on a flat plate, J. Colloid Interface Sci. 61 (1977) 77–85.
[5] G.K. Batchelor, C. Shen, Thermophoretic deposition of particles in gas flowing over cold surfaces, J. Colloid Interface Sci. 107 (1985) 21–37.
[6] C. Shen, Thermophoretic deposition of particles onto cold surfaces of bodies in two-dimensional and axisymmetric flows, J. Colloid Interface Sci. 127 (1) (1989) 104–115.
[7] G.M. Homsy, F.T. Geyling, K.L. Walker, Blasius series for thermophoretic deposition of small particles, J. Colloid Interface Sci. 83 (1981) 495–501.
[8] K.L. Walker, G.M. Homsy, F.T. Geyling, Thermophoretic deposition of small particles in laminar tube flow, J. Colloid Interface Sci. 69 (1979) 138–147.
[9] T. Li (Ed.), Optical Fiber Communications, Vol. 1: Fiber Fabrication, Academic Press, 1985.
[10] D.E. Rosner, Combustion synthesis and materials processing, Chem. Eng. Educ. (Fall) (1997) 228–235.
[11] K. Hong, S. Kang, Three-dimensional analysis of heat transfer and thermophoretic particle deposition in OVD process, Int. J. Heat Mass Transfer 41 (1998) 1339–1346.
[12] J. Cho, J. Kim, M. Choi, An experimental study of mass transfer and particle deposition during the outside vapor deposition process, Int. J. Heat Mass Transfer 41 (1998) 435–445.
[13] C.K. Wu, R. Grief, Thermophoretic deposition including an application to the outside vapor deposition process, Int. J. Heat Mass Transfer 39 (1996) 1429–1438.
[14] K.S. Park, M. Choi, J.D. Chung, Unsteady heat and mass transfer on the codeposition of SiO_2/GeO_2 during the modified chemical vapor deposition process, Int. J. Heat Mass Transfer 43 (2000) 3209–3217.
[15] K.S. Park, M. Choi, Conjugate heat transfer and particle deposition in the modified chemical vapor deposition process: effects of torch speed and solid layer, Int. J. Heat Mass Transfer 37 (1994) 1593–1603.
[16] K.S. Park, M. Choi, Analysis of unsteady heat transfer and mass transfer during the modified chemical vapor deposition process, Trans. ASME 120 (1998) 858–864.
[17] K.S. Kim, S.E. Pratsinis, Manufacture of optical waveguide preforms by MCVD, AIChE J. 34 (1988) 912–920.
[18] G.M. Graham, M.K. Alam, Experimental study of the outside vapor deposition process, Aerosol Sci. Technol. 15 (1991) 69–76.
[19] J.R. Bautista, K.L. Walker, R.M. Atkins, Modeling heat and mass transfer in optical waveguide manufacture, Chem. Eng. Prog. (Feb) (1990) 47–52.
[20] A.D. Eisner, D.E. Rosner, Experimental studies of soot particle thermophoresis in nonisothermal combustion gases using thermocouple response technique, Combust. Flame 61 (1985) 153–166.
[21] C.S. McEnally, U.O. Koylu, L.D. Pfefferle, D.E. Rosner, Soot volume fraction and temperature measurements in laminar nonpremixed flames using thermocouples, Combust. Flame 109 (1997) 701–720.
[22] H.M. Park, D.E. Rosner, Combined inertial and thermophoretic effects on particle deposition rates in highly loaded dusty gas systems, Chem. Eng. Sci. 44 (10) (1989) 2233–2244.
[23] D.E. Rosner, H.M. Park, Thermophoretically augmented mass-, momentum-, and energy transfer rates in high particle mass-loaded laminar forced convection systems, Chem. Eng. Sci. 43 (1988) 2689.
[24] P. Tandon, J. Balakrishnan, Predicting heat transfer to a growing, rotating preform during outside vapor deposition process, prepared for submission.
[25] A. Gomez, D.E. Rosner, Thermophoretic effects on particles in counterflow diffusion flames, Combust. Sci. Technol. 89 (1993) 335–362.
[26] P. Tandon, D.E. Rosner, Codeposition on hot CVD surfaces: particle dynamics and deposit roughness interactions, AIChE J. 42 (6) (1996) 1673–1684.
[27] P. Tandon, D.E. Rosner, Heat transfer properties of large multi-particle aggregates: pseudo-continuum estimation/correlation of orientation-averaged Nusselt number, AIChE Annual Mtg., Chicago, 1996.

[28] L. Waldmann, K.H. Schmitt, Thermophoresis and diffusiophoresis of aerosols, in: C.N. Davies (Ed.), Aerosol Science, Academic Press, New York, 1966, pp. 137–162, Chapter 6.
[29] D.R. Powers, Kinetics of $SiCl_4$ oxidation, J. Am. Ceram. Soc. 61 (1978) 295.
[30] D.L. Wood, J.B. MacChesney, J.P. Luongo, Investigation of the reactions of $SiCl_4$ and O_2 at elevated temperatures by infra-red spectroscopy, J. Mater. Sci. 13 (1978) 1761–1768.
[31] J.M. Hager, J.P. Terrell, L.W. Langley, S. Onishi, T.E. Diller, Measurements with the heat flux microsensor, 37th International Instrumentation Symposium, ISA, May 5–9, 1991.
[32] M.R. Zachariah, D. Chin, H.G. Semerjian, J.L. Katz, Silica particle synthesis in a counterflow diffusion flame reactor, Combust. Flame 78 (1989) 287–298.
[33] T.T. Charalampopoulos, Morphology and dynamics of agglomerated particulates in combustion systems using light scattering techniques, Prog. Energy Combust. Sci. 18 (1992) 13–45.
[34] Y. Xing, U.O. Koylu, D.E. Rosner, In-situ light scattering measurements of morphologically evolving flame synthesized oxide nano-aggregates, Appl. Opt. 38 (12) (1999) 2686–2697.
[35] Y. Xing, D.E. Rosner, U.O. Koylu, P. Tandon, Morphological evolution of nanoparticles in diffusion flames: measurement and modeling, AIChE J. 43 (11) (1997) 2641–2649.
[36] P.W. Barber, S.C. Hill, Light Scattering by Particles: Computational Methods, World Scientific Publication Co, Singapore, 1990.
[37] A.G. Konstandopoulos, D.E. Rosner, Inertial effects on thermophoretic transport of small particles to walls with streamline curvature, Int. J. Heat Mass Transfer 38 (12) (1995) 2305–2327.
[38] D.E. Rosner, P. Tandon, Rational prediction of inertially induced particle deposition rates for a cylindrical target in a dust-laden stream, Chem. Eng. Sci. 50 (1995) 3409–3431.
[39] D.E. Rosner, D.W. Mackowski, P. Garcia-Ybarra, Size and structure insensitivity of the thermophoretic transport of aggregated soot particles in gases, Combust. Sci. Tech. 80 (1991) 87–101.